

Microfabrics of omphacite and garnet in eclogite from the Lanterman Range, northern Victoria Land, Antarctica

Daeyeong Kim^{1*}, Tachwan Kim², Jeongmin Lee¹, Yoonsup Kim³, Hyeoncheol Kim⁴, and Jong Ik Lee⁵

¹Division of Polar Earth-System Sciences, Korea Polar Research Institute (KOPRI), Incheon 21990, Republic of Korea

²School of Earth and Environmental Sciences, Seoul National University, Seoul 08826, Republic of Korea

³Department of Geology and Earth Environmental Sciences, Chungbuk National University, Cheongju 28644, Republic of Korea

⁴Geology Division, Korea Institute of Geoscience and Mineral Resources (KIGAM), Daejeon 34132, Republic of Korea

⁵Unit of Antarctic K-route Expedition, Korea Polar Research Institute (KOPRI), Incheon 21990, Republic of Korea

ABSTRACT: We examined the microfabrics of omphacite and garnet in foliated eclogite to determine the influence of the layered structure on seismic observations in subduction zone. The analyzed eclogite, from the Lanterman Range, northern Victoria Land, Antarctica, is characterized by layering in which the modal abundances of garnet and omphacite vary. For garnet, the low aspect ratios, similar angular distribution of long axes relative to the foliation in both layers, uniform grain size distribution, near-random crystallographic preferred orientations (CPOs), and misorientation angle distributions are indicative of passive behavior during deformation. In contrast, omphacite shows relatively high aspect ratios, a low angle between the long axes of crystals and the foliation, a wide grain-size distribution, and distinctive CPOs, suggesting dislocation creep as the main deformation mechanism. The results of fabric analyses are consistent with strain localization into omphacite or omphacite-rich layers rather than garnet or garnet-rich layers. The single-crystal seismic anisotropy of garnet is very weak ($AV_p = 0.2\%$, $AV_s = 0.5\text{--}0.6\%$), whereas that of omphacite is much stronger ($AV_p = 3.7\text{--}5.9\%$ and $AV_s = 2.9\text{--}3.8\%$). Seismic anisotropy of the omphacite-rich layers shows an increase of 329% for AV_p and 146% for AV_s relative to the garnet-rich layers. Our results demonstrate the importance of the layered structure in strain localization and in the development of the seismic anisotropies of subducting oceanic crust.

Key words: eclogite, omphacite, garnet, layered structure, seismic anisotropy, electron backscatter diffraction (EBSD)

Manuscript received July 13, 2018; Manuscript accepted September 17, 2018

1. INTRODUCTION

Microstructures within high-pressure metamorphic rocks such as blueschists and eclogites provide insights into the mechanisms of subduction-zone deformation (e.g., Godard, 2001). Internal structures of subduction zone are often identified by seismic observations on shear wave splitting which can be computed from seismic properties of minerals and rocks based on crystallographic preferred orientation (CPO) data (e.g., Ji et al., 2003; Morales and Tommasi, 2011). Recent studies on the microstructures of subduction-zone metamorphic rocks have concentrated on particular phases (e.g., glaucophane, lawsonite,

omphacite) with regard to the rheology and seismic properties of high-pressure metamorphic rocks (Bascou et al., 2001; Zhang and Green, 2007; Bezacier et al., 2010; Fujimoto et al., 2010; Kim et al., 2013a, b; Cao et al., 2014; Cao and Jung, 2016; Kim et al., 2016; Ha et al., 2018). In particular, lawsonite in blueschists controls the rheology of lawsonite-rich layers and significantly decreases the seismic anisotropy of the bulk rock (Kim et al., 2013a), indicating the important role of primary layering in the deformation of subducting oceanic crust. Layered structures in eclogites are commonly formed during exhumation in a subduction channel (e.g., Whitney et al., 2014; Keppler et al., 2015, 2016), although there is little published data on the layered structures formed during subducting processes.

The single-crystal seismic anisotropy of garnet (< 1%) is weaker than that of omphacite (up to ~20% for P-wave seismic anisotropy and ~15% for S-wave seismic anisotropy; Bascou et al., 2001). The seismic anisotropy of eclogite is generally reported to be less than ~5%, which can be ascribed predominantly to the properties

*Corresponding author:

Daeyeong Kim

Division of Polar Earth-System Sciences, Korea Polar Research Institute (KOPRI), 26 Songdomirae-ro, Yeosu-gu, Incheon 21990, Republic of Korea
Tel: +82-32-760-5443, Fax: +82-32-770-5494, E-mail: dkim@kopri.re.kr

©The Association of Korean Geoscience Societies and Springer 2018

of omphacite (Bascou et al., 2001, 2002; Zhang et al., 2008; Ábalos et al., 2011; Cao et al., 2013; Worthington et al., 2013). Here we report the microstructures of a pristine eclogite that contains alternating garnet- and omphacite-rich layers from northern Victoria Land (NVL) in Antarctica. In addition, we discuss the rheological contrast between garnet and omphacite, and its implications for the seismic properties of rocks on the basis of fabric analyses combined with modeled geochemical data.

2. GEOLOGICAL BACKGROUND

The Transantarctic Mountains in NVL, Antarctica, formed during the Ross–Delamerian Orogeny that resulted from convergence between the Paleo-Pacific oceanic lithosphere and the continental margin of Gondwana during the Cambrian to Ordovician. Across the orogen, three accretionary terranes are recognized, from northeast to southwest (e.g., Bradshaw and Laird,

1983): the Robertson Bay Terrane, consisting of a thick, folded flysch-type sequence of low-grade late Cambrian–Ordovician sedimentary rocks; the Bowers Terrane, comprising Cambrian metavolcanic rocks and related sediments (Weaver et al., 1984); and the Wilson Terrane, characterized by low- and medium- to high-grade metasedimentary rocks that are widely intruded by the Granite Harbour Intrusives, which have a calc-alkaline affinity (Armienti et al., 1990; Rocchi et al., 1998; Bomparola et al., 2007) (Fig. 1). The Lanterman Range, situated at the boundary between the Bowers and Wilson terranes, contains eclogite boudins or lenses enveloped by quartzofeldspathic gneisses/schists (Ricci et al., 1996, 1997; Di Vincenzo et al., 1997; Talarico et al., 1998; Ghiribelli et al., 2002; Palmeri et al., 2009, 2011). Clockwise peak-to-retrograde pressure-temperature path is recorded within the retrogressed eclogites or eclogitic amphibolites, including an eclogite facies stage characterized by omphacite-garnet-rutile-bearing assemblages together with quartz/coesite. A medium-

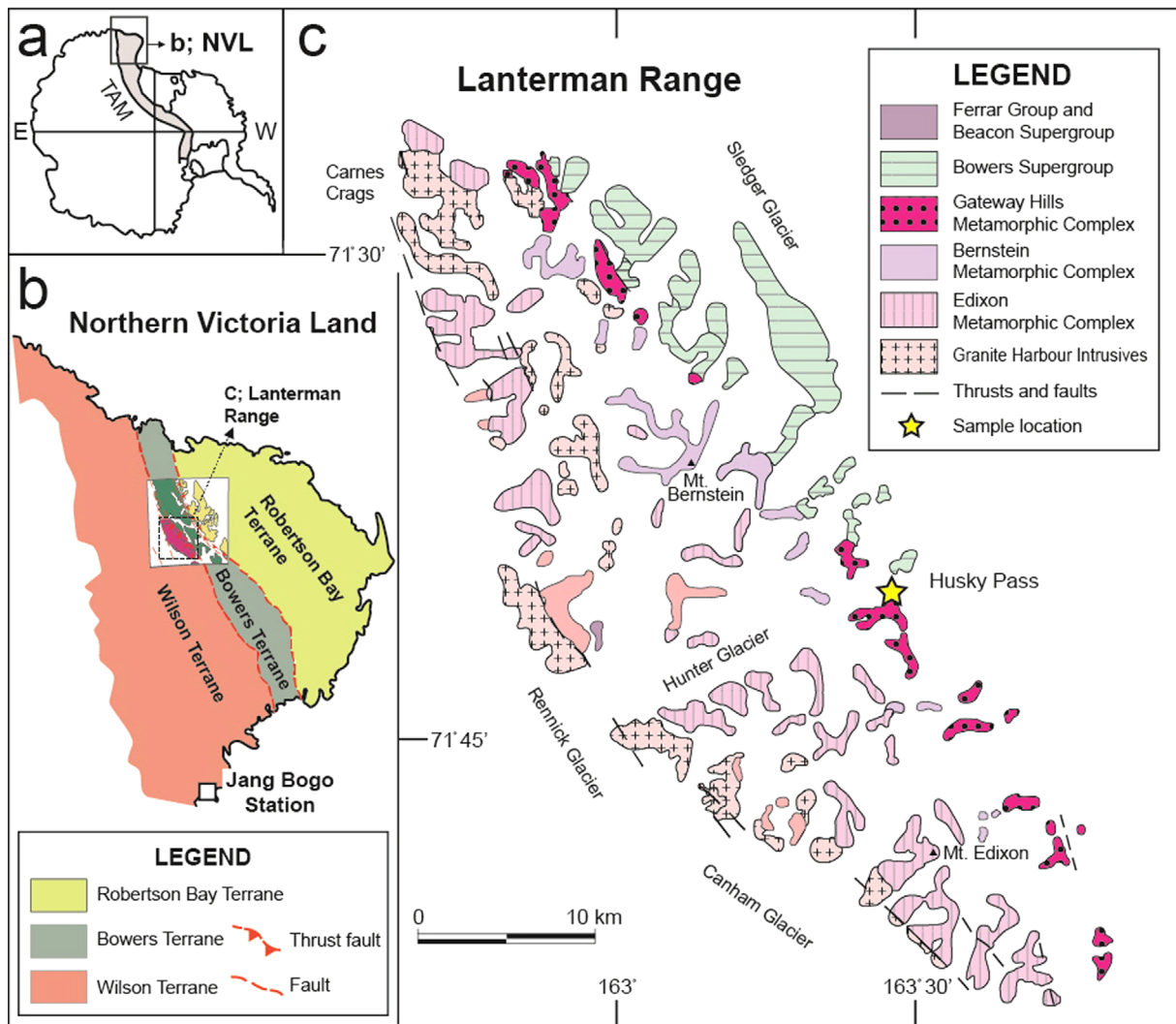


Fig. 1. Geologic map of the Lanterman Range, northern Victoria Land (NVL), Antarctica, showing the location of the studied eclogite sample. Modified from Di Vincenzo and Palmeri (2001).

pressure amphibolite facies stage is distinguished by symplectitic intergrowths of Na-poor clinopyroxene and albite-rich plagioclase along with barroisite, and a low-pressure amphibolite facies typically characterized by the pervasive development of amphibole (Di Vincenzo et al., 1997). Two distinct eclogitization events are reported. The high- to ultrahigh-pressure prograde/peak metamorphism forming medium-grained and undeformed eclogites took place at ~530 Ma during an active continental margin stage with pressure-temperature conditions of 1.7–2.4 GPa and 700 °C (Di Vincenzo et al., 2016). Finer-grained and slightly deformed eclogites formed at 500 Ma during the subsequent island arc-continental arc collision with temperature conditions of ~800 °C (Di Vincenzo et al., 1997; Ghiribelli et al., 2002; Palmeri et al., 2007, 2011). The eclogitizations were followed by exhumation first to mantle depths (30–40 km at ~490 Ma) and then to shallow crustal levels (at ~480 Ma) (Di Vincenzo et al., 2001; Crispini et al., 2007; Godard and Palmeri, 2013). Based on overlapping Sm-Nd, U-Pb, and Ar-Ar ages, rapid cooling rates of ~3–4 mm/yr were inferred (e.g., Di Vincenzo and Palmeri, 2001). The geochemical and Nb isotope of well-preserved eclogites and whole-rock compositions of retrogressed eclogites suggest that they are derived from a different mantle source with an enriched signature and a depleted mantle, respectively (Di Vincenzo et al., 1997).

3. SAMPLE DESCRIPTION

Eclogite from the Lanterman Range, NVL, Antarctica, commonly occurs as centimeter- to decimeter-sized pods and lenses within quartzofeldspathic gneisses. Samples of variably deformed eclogites in the Husky Pass region of the Lanterman Range (71°40′47.16″S, 163°27′28.56″E; Fig. 1) were collected during the 2014–2015 Korean Antarctic mission. We analyzed a medium-grained pristine eclogite sample that is characterized by alternating garnet-rich (69 vol%) and omphacite-rich (75 vol%) layers (Fig. 2). The peak assemblage (garnet + omphacite + amphibole + rutile + quartz ± epidote) shows only limited retrograde metamorphism in the form of small amounts of symplectitic plagioclase-clinopyroxene and rarely plagioclase-amphibole intergrowths after omphacite. Both garnet- and omphacite-rich layers (GRL and ORL, respectively) are composed primarily of idio- to hypidioblastic garnet and omphacite, and hypidio- to xenoblastic amphibole and epidote, together with minor amounts of rutile, ilmenite, titanite, and quartz, and accessory zircon and allanite. Most of the minerals are aligned parallel to the dominant foliation, except garnet and some of amphibole and symplectite. Garnet in both layers is broadly equidimensional and contains inclusions of amphibole, epidote, rutile, plagioclase, and quartz. Omphacite often having

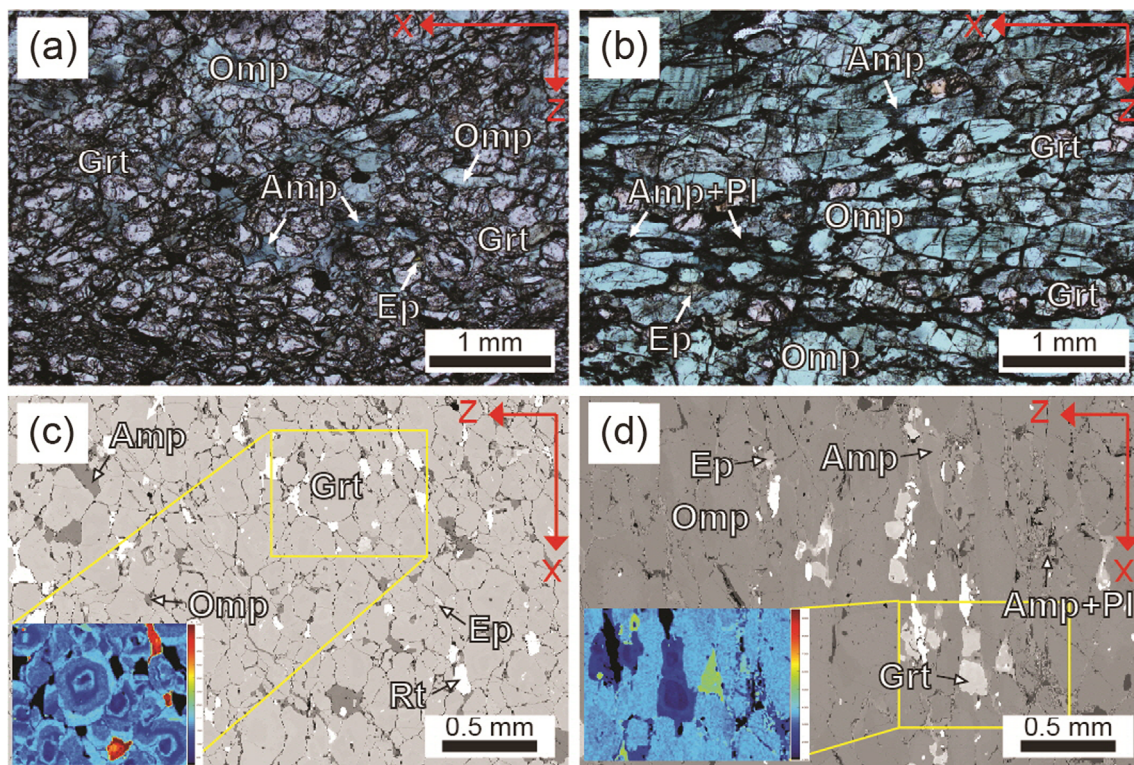


Fig. 2. Photomicrographs and back-scattered electron images (BSEIs) of garnet- and omphacite-rich layers (GRL: a and c; ORL: b and d). The insets in c and d are Ca X-ray composition maps of the areas indicated by yellow rectangles. Mineral abbreviations are after Whitney and Evans (2010).

intracrystalline deformation feature (undulose extinction) is hypidid- to xenoblastic in the GRL, but idioblastic in the ORL. Statistical comparisons of the mineralogical layering defined mainly by garnet and omphacite would provide an opportunity to understand the mechanical behavior of each mineral and assess the effects on seismic properties in the deep Earth (e.g., Kim et al., 2013a).

4. ANALYTICAL TECHNIQUES

The chemical compositions of representative minerals were measured using a JXA-8530 field emission electron probe microanalyzer at the Korea Polar Research Institute, Incheon, Korea. Point analysis and X-ray maps were collected using an accelerating voltage of 15 kV, a beam current of 10 nA, and a beam diameter of 5 μm . Natural silicates were used as standards, and matrix corrections were calculated using a ZAF correction program. The proportion of Fe^{3+} in amphiboles was estimated using an average based on a total of 13 cations for the T sites and 15 cations for the T, C, B sites (Leake et al., 1997).

The CPOs of garnet and omphacite were measured in thin sections cut normal to the foliation and parallel to the lineation (XZ sections), by automatic indexing of electron backscatter diffraction (EBSD) patterns using an Oxford-HKL-EBSD on a JEOL JSM-7100F field emission-scanning electron microscope housed at the Korea Institute for Rare Metals, Incheon, Korea. After mechanical and chemical polishing, samples were coated with a thin layer of carbon (~10 nm) to prevent charging. The measurements used an accelerating voltage of 20 kV, a step size of 30 μm , and a working distance of ~20 mm. The software 'AZtec'

was used to compile montaged maps, and 'PFctf' was used to plot crystallographic orientation data on lower-hemisphere equal-area projections (Mainprice, 1990). To estimate fabric strength, the *M*- and *J*-indices were calculated using the Matlab-based toolbox 'MTEX' (Bunge, 1982; Mainprice and Silver, 1993; Skemer et al., 2005; Mainprice et al., 2011).

The seismic properties of garnet and omphacite, and of fictive whole rocks made from these minerals were calculated based on the EBSD data and modal abundances of phases in both layers (Mainprice, 1990; Mainprice et al., 2000). The P-wave seismic anisotropy (AV_p) is usually defined as the difference between the maximum and minimum velocities in two dissimilar propagating paths, and hence can be calculated using the formula $200(V_{p_{\text{max}}} - V_{p_{\text{min}}}) / (V_{p_{\text{max}}} + V_{p_{\text{min}}})$. The S-wave seismic anisotropy (AV_s) is normally defined as the difference between two dissimilar velocities of two orthogonally polarized S-waves individually propagating through an anisotropic medium. Thus, the percentage AV_s can be computed as $200(V_{s1} - V_{s2}) / (V_{s1} + V_{s2})$, in which V_{s1} and V_{s2} are the faster and slower velocities, respectively. Seismic properties were computed using the program 'ANISctf' (Mainprice, 1990) and the Matlab-based toolbox MTEX (Mainprice et al., 2011). For calculating seismic properties, we employed the densities and respective single crystal elastic constants (C_{ij}) of pyrope (Babuška et al., 1978) and omphacite (Bhagat et al., 1992) using the Voigt-Reuss-Hill averaging scheme.

5. RESULTS

The composition of garnet in the foliated eclogite is characterized by fluctuating grossular contents with X_{Grs} ($= \text{Ca} / (\text{Fe}^{2+} + \text{Mn} +$

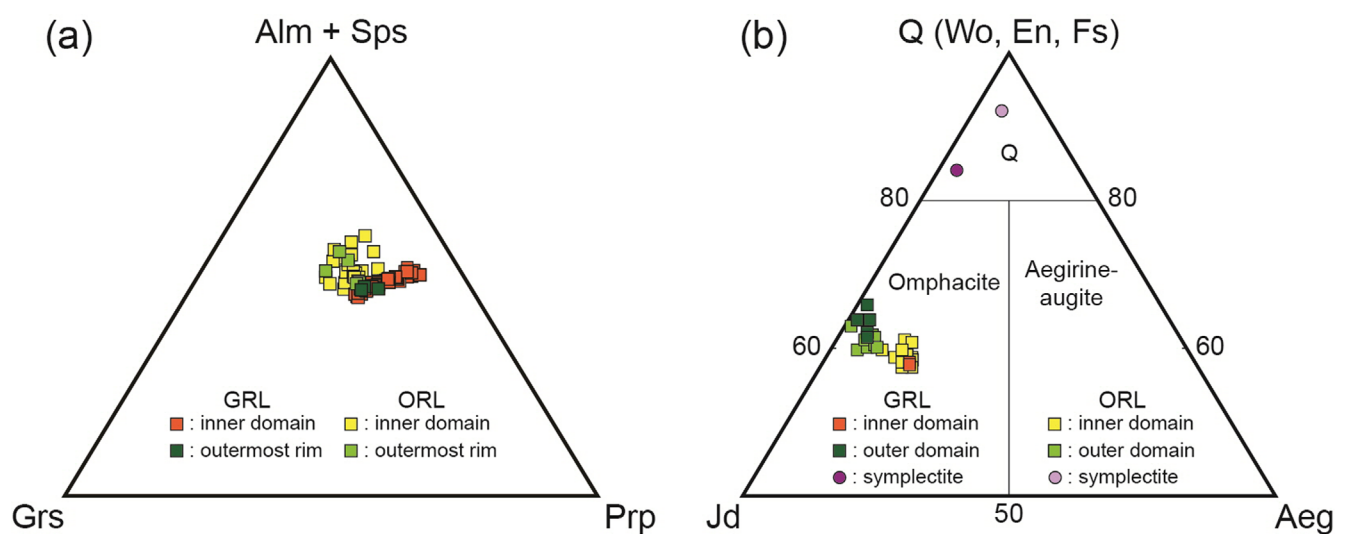


Fig. 3. Compositional classification diagrams for garnet (a) and clinopyroxene (b) from the garnet- and omphacite-rich layers (GRL and ORL, respectively) in the foliated eclogite. (a) An (almandine + spessartine)-grossular-pyrope ternary plot. (b) Quadrilateral clinopyroxene-jadeite-aegirine ternary plot (after Morimoto et al., 1988). Mineral and end-member abbreviations are after Whitney and Evans (2010); p.f.u. = per formula unit; Q = quadrilateral clinopyroxene.

Table 1. Chemical compositions of representative minerals in pristine eclogite

Mineral	Garnet-rich Layer										Omphacite-rich Layer																		
	Grt					Omp					Pl					Grt					Omp					Pl			
Spot No. ^(a)	4-4C	4-4R	01-01C	01-01R	7S	6-5C	6-5R	Amp	5S	7S	6C	6R	9-5C	9-5R	3S	8-3C	8-3R	Amp	1S	5S									
SiO ₂	38.95	39.01	54.66	55.21	52.88	49.16	46.46	48.70	65.62	38.92	38.47	54.26	55.01	54.44	48.67	48.95	45.82	67.30											
TiO ₂	0.05	0.30	0.12	0.15	0.18	0.22	0.28	0.33	0.02	0.05	0.14	0.15	0.12	0.02	0.30	0.25	0.49	0.00											
Al ₂ O ₃	21.66	21.43	7.32	8.42	3.60	9.90	13.21	10.79	21.73	21.34	21.13	7.39	8.09	0.92	10.17	8.58	9.93	20.29											
Cr ₂ O ₃	0.03	0.03	0.11	0.04	0.07	0.03	0.00	0.09	0.00	0.00	0.01	0.00	0.06	0.01	0.10	0.04	0.11	0.00											
FeO ^b	22.88	20.92	8.59	5.85	7.56	8.71	8.93	9.49	0.44	23.12	22.69	8.06	6.40	6.27	11.05	11.70	11.79	0.30											
MnO	2.00	1.94	0.09	0.08	0.19	0.13	0.17	0.13	0.00	1.23	1.33	0.07	0.05	0.14	0.17	0.06	0.20	0.02											
MgO	10.10	8.15	8.75	9.62	12.40	15.69	14.55	14.66	0.02	7.91	6.28	9.27	9.54	14.38	14.09	14.60	13.58	0.02											
CaO	3.67	7.46	14.34	15.49	20.11	8.93	9.33	9.09	2.78	7.12	9.30	14.61	15.13	22.59	8.82	9.73	11.23	1.36											
Na ₂ O	0.01	0.00	5.84	5.39	2.12	2.79	3.16	2.97	9.97	0.03	0.00	5.63	5.46	1.06	3.25	2.74	2.48	10.64											
K ₂ O	0.02	0.00	0.00	0.00	0.01	0.22	0.03	0.01	0.01	0.00	0.00	0.00	0.00	0.00	0.11	0.00	0.00	0.00											
Total	99.37	99.24	99.81	100.24	99.13	95.78	96.13	96.26	100.58	99.72	99.34	99.44	99.85	99.83	96.73	96.65	95.63	99.93											
<i>Cations</i>	O = 12	O = 12	O = 6	O = 6	O = 6	O = 23	O = 23	O = 23	O = 8	O = 12	O = 12	O = 6	O = 6	O = 6	O = 23	O = 23	O = 23	O = 8											
Si	2.99	3.01	1.98	1.98	1.99	7.03	6.66	6.96	2.87	3.00	2.99	1.98	1.98	2.01	6.98	7.06	6.78	2.95											
Ti	0.00	0.02	0.00	0.00	0.00	0.02	0.03	0.04	0.00	0.00	0.01	0.00	0.00	0.00	0.03	0.03	0.05	0.00											
Al	1.96	1.95	0.31	0.36	0.16	1.67	2.23	1.82	1.12	1.94	1.94	0.32	0.34	0.04	1.72	1.46	1.73	1.05											
Cr	0.00	0.00	0.00	0.00	0.00	0.00	0.00	0.01	0.00	0.00	0.00	0.00	0.00	0.00	0.01	0.00	0.01	0.00											
Fe ³⁺	0.04	0.03	0.09	0.02	0.00	0.43	0.41	0.36	-	0.07	0.07	0.08	0.04	0.04	0.38	0.38	0.20	-											
Fe ²⁺	1.43	1.32	0.17	0.16	0.23	0.61	0.66	0.78	0.02	1.42	1.41	0.17	0.16	0.16	0.94	1.03	1.26	0.01											
Mn	0.13	0.13	0.00	0.00	0.01	0.02	0.02	0.02	0.00	0.08	0.09	0.00	0.00	0.00	0.02	0.01	0.03	0.00											
Mg	1.16	0.94	0.47	0.51	0.69	3.34	3.11	3.13	0.00	0.91	0.73	0.50	0.51	0.79	3.01	3.14	3.00	0.00											
Ca	0.30	0.62	0.56	0.59	0.80	1.37	1.43	1.39	0.13	0.59	0.77	0.57	0.58	0.89	1.36	1.50	1.78	0.06											
Na	0.00	0.00	0.41	0.37	0.15	0.77	0.88	0.82	0.85	0.00	0.00	0.40	0.38	0.08	0.90	0.77	0.71	0.90											
K	0.00	0.00	0.00	0.00	0.00	0.04	0.01	0.00	0.00	0.00	0.00	0.00	0.00	0.00	0.02	0.00	0.00	0.00											
Total	8.02	8.00	4.00	4.01	3.99	15.30	15.43	15.32	4.99	8.00	8.00	4.01	4.00	4.01	15.39	15.38	15.55	4.98											
Fe ²⁺ /(Fe ²⁺ + Mg)	0.55	0.58	0.26	0.23	0.25	0.15	0.18	0.20	-	0.61	0.66	0.24	0.23	0.17	0.24	0.25	0.30	-											
Na/(Ca + Na)	-	-	0.41	0.38	0.16	0.36	0.38	0.37	0.87	-	-	0.40	0.38	0.08	0.40	0.34	0.29	0.93											

^(a)C, R, and S in spot numbers indicate core, rim, and symplectite, respectively.
^(b)FeO^b denotes total Fe.

Mg + Ca) = 0.08–0.22 and 0.15–0.26 for the GRL and ORL, respectively (Fig. 3a; Table 1), and relatively uniform spessartine contents ($X_{\text{Sps}} = \text{Mn}/(\text{Fe}^{2+} + \text{Mn} + \text{Mg} + \text{Ca}) < 0.05$). Domains with high grossular contents are notably parallel to the foliation (Figs. 2c and d). The X_{Fe} value ($= \text{Fe}^{2+}/(\text{Fe}^{2+} + \text{Mg})$) of garnet increases from core to rim in both the GRL (0.54–0.58) and ORL (0.57–0.65). A slight Fe enrichment owing to diffusional re-equilibration is evident in a narrow outermost rim ($X_{\text{Fe}} = 0.58$ –0.59 for the GRL and 0.66–0.68 for the ORL). Omphacite is zoned from aegirine-rich cores ($\text{Fe}^{3+} = 0.04$ –0.09) to aegirine-poorer rims ($\text{Fe}^{3+} = 0.01$ –0.04), in which the aegirine content is generally complementary to the jadeite content (Fig. 3b; Table 1). The X_{Fe} of omphacite is rather constant throughout each grain, but is slightly higher in the GRL (0.22–0.26) than in the ORL (0.20–0.25). The symplectitic clinopyroxene at the margins of omphacite is diopside in composition ($X_{\text{Na}} = \text{Na}/(\text{Na} + \text{Ca}) = 0.08$ –0.16). Hypidio- to xenoblastic amphibole is dominated by barroisite and Mg-hornblende (amphibole nomenclature after Leake et al., 1997), and retrograde amphibole intergrown with plagioclase is Mg-hornblende in composition. Epidote xenoblasts in the matrix vary in $X_{\text{Ep}} (= (\text{Al}^{\text{VI}} - 2)/(\text{Al}^{\text{VI}} + \text{Fe}^{3+} - 2))$ value from 0.53 to 0.61. Vermicular plagioclase replacing omphacite is albite to oligoclase ($X_{\text{Na}} = 0.87$ –0.93).

Image analyses on XZ sections were conducted to quantify the fabrics. The best-fit ellipses (using ImageJ 1.51) were adopted to reduce the complexity of the various grain shapes and to quantify the aspect ratio, orientation of long axes relative to the foliation, and the area of each crystal (e.g., Mezger, 2010; Kim et al., 2013a). Grain size was calculated as the area of a circle with the same internal area as the calculated best-fit ellipse. Garnet in both layers is euhedral to subhedral with a mean aspect ratio of 1.7, and shows a shape preferred orientation relative to the foliation without any change in both layers, and a relatively uniform grain size with a small standard deviation (85 – 98 ± 34 – $44 \mu\text{m}$) (Fig. 4; Table 2). In contrast, omphacite in the ORL exhibits a higher aspect ratio of 2.9 ± 1.3 , a lower angle relative to the foliation particularly distinct in the ORL, and a larger mean grain size of $98 \pm 65 \mu\text{m}$ compared with the GRL. The variable results for garnet and omphacite are probably due to their different behaviors during deformation.

Garnet in the analyzed eclogite displays a near-random CPO (0.002 for the M -index and 1.031–1.028 for the J -index: Figs. 5a, b and Table 2). However, omphacite shows a CPO that is distinguished by being lineation-subparallel [001] axes and foliation-parallel (010) planes (Figs. 5c and d). The omphacite fabric in the ORL ($M = 0.207$, $J = 7.162$) is stronger than that in

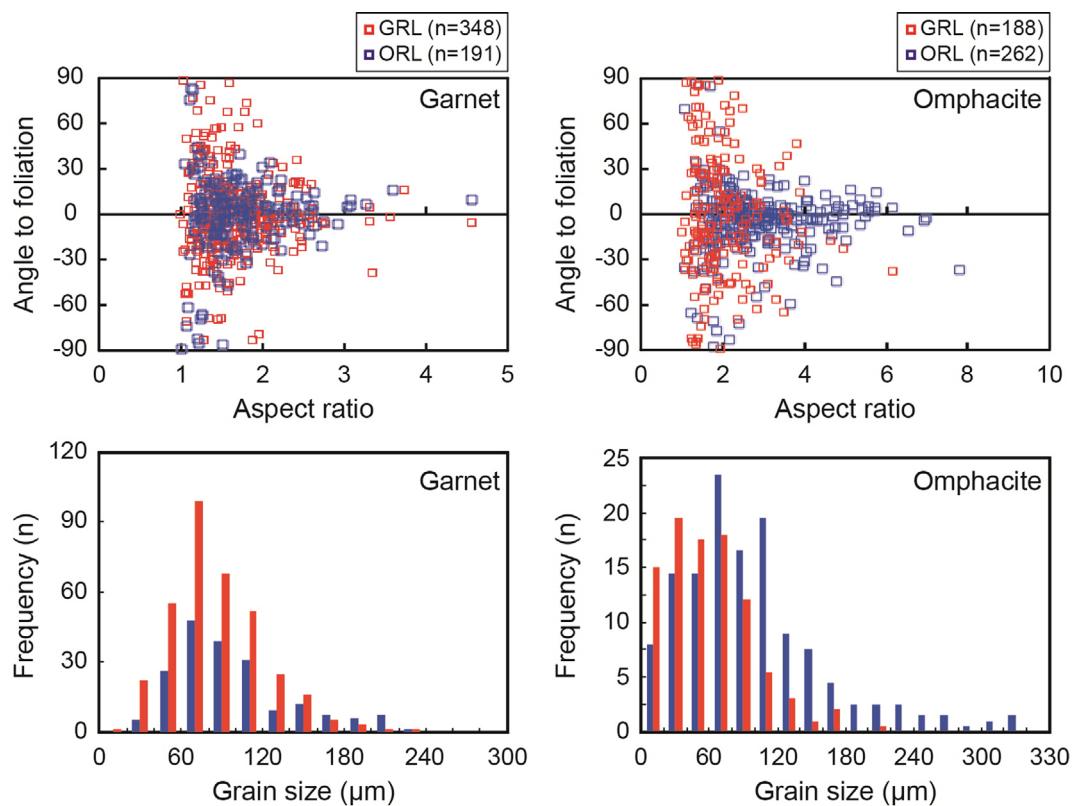


Fig. 4. Angle between crystal long axes and the foliation versus the aspect ratio, and grain size distributions for garnet and omphacite, on the basis of image analyses on XZ sections. Garnet tends to have a small range of aspect ratios and a small distribution of grain size, whereas omphacite shows higher angles between crystal long axes and the foliation in the ORL and bi- to trimodal grain-size distributions in both layers.

Table 2. Results of fabric analysis

Sample numbers	Location (latitude, longitude)	Mode (%) ^(a)	Minerals	Bulk-rock composition ^(b)	Grain size with std. dev. (μm)	Aspect ratio with std. dev.	Fabric strength (CPO)			Seismic anisotropy (%)	
							Number	M	J	AV_p	AV_s
GRL	71°40' 47.16"S, 163°27' 28.56"E	Grt69, Omp10, Amp10, Ep8	Grt Omp	SiO ₂ 40, Al ₂ O ₃ 22, FeO 21, MnO 2, MgO 9, CaO 6	85 ± 34	1.7 ± 0.5	37047	0.0015	1.0309	0.2	0.50
					59 ± 39	2.0 ± 0.8	3175	0.1019	6.5731	5.9	2.86
ORL		Omp75, Grt15, Amp7	Grt Omp	SiO ₂ 56, Al ₂ O ₃ 8, FeO 7, MgO 9, CaO 14, Na ₂ O 5	98 ± 44	1.7 ± 0.5	6603	0.0015	1.0278	0.2	0.64
					98 ± 65	2.9 ± 1.3	57962	0.2070	7.1624	3.7	3.77

^(a)Mode excludes epidote, rutile, ilmenite, quartz, zircon, allanite and titanite (abundances of each mineral are less than 5%).

^(b)100% normalized bulk-rock composition is calculated based on elemental maps acquired by a FE-EPMA. Mineral abbreviations follow Whitney and Evans (2010).

Number: number of measurements; M: M-index; J: J-index.

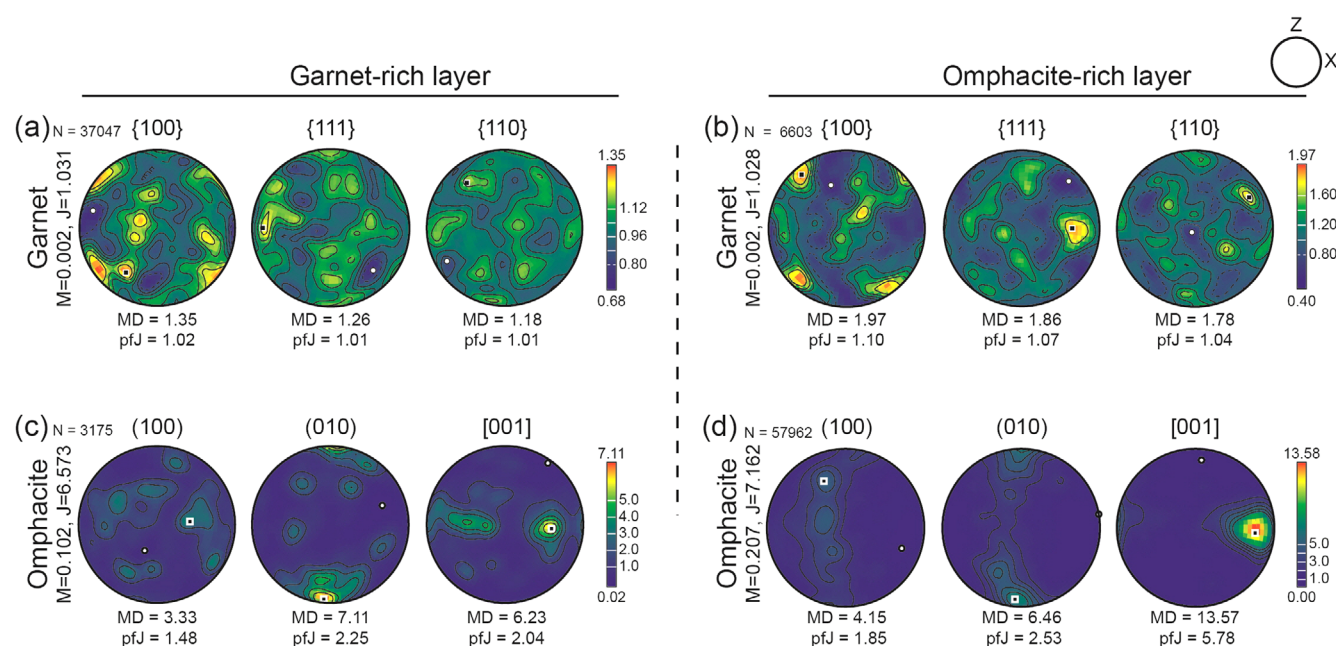


Fig. 5. Crystal preferred orientations (CPOs) of garnet and omphacite from each layer (equal area, lower hemisphere projections). N: number of analysis points; M: M-index; J: J-index; MD: mean density; pfJ: pole figure J-index; X: lineation; Z: foliation normal.

the GRL ($M = 0.102$, $J = 6.573$), which is consistent with the results of image analysis that indicate a larger grain size, higher aspect ratio, and lower angle to foliation in the ORL compared with the GRL. Based on the concentration of [001] subparallel to the lineation (Fig. 5d), omphacite CPOs in the ORL are L-type, indicative of constrictional strain (e.g., Helmstaedt et al., 1972; Godard and van Roermund, 1995; Kurz et al., 2004). Misorientations of uncorrelated garnet grains correspond to a random pattern, whereas those of omphacite are not random (Fig. 6). The misorientation angle distributions of both minerals are more random in the GRL than in the ORL.

The seismic properties of garnet polycrystals, calculated based on EBSD data, exhibit V_p maxima parallel to the foliation and normal to the lineation, and AV_s maxima parallel and normal to both the foliation and lineation (Fig. 7). The weak AV_p (~0.2%) and AV_s (0.5–0.6%) of garnet in both layers suggest a negligible influence of single crystals on the seismic

properties of the rock (i.e., eclogite). Omphacite shows V_p maxima parallel to the lineation, which is relatively strong ($AV_p = 3.7$ – 5.9%) in both layers. The AV_s of omphacite develops variably and the V_{S1} (fast S-wave velocity) polarization is developed oblique to the foliation. The P- and S-wave anisotropy patterns of bulk rocks, computed based on the assumption that the rock is composed only of garnet and omphacite, show similar patterns to those of omphacite, and the seismic properties in the ORL are stronger than those in the GRL (Fig. 8).

6. DISCUSSION

6.1. Geochemistry of the GRL and ORL, and P-T Conditions

To understand the origin of the GRL and ORL due to difficulty for measuring chemical composition of each layer directly, we

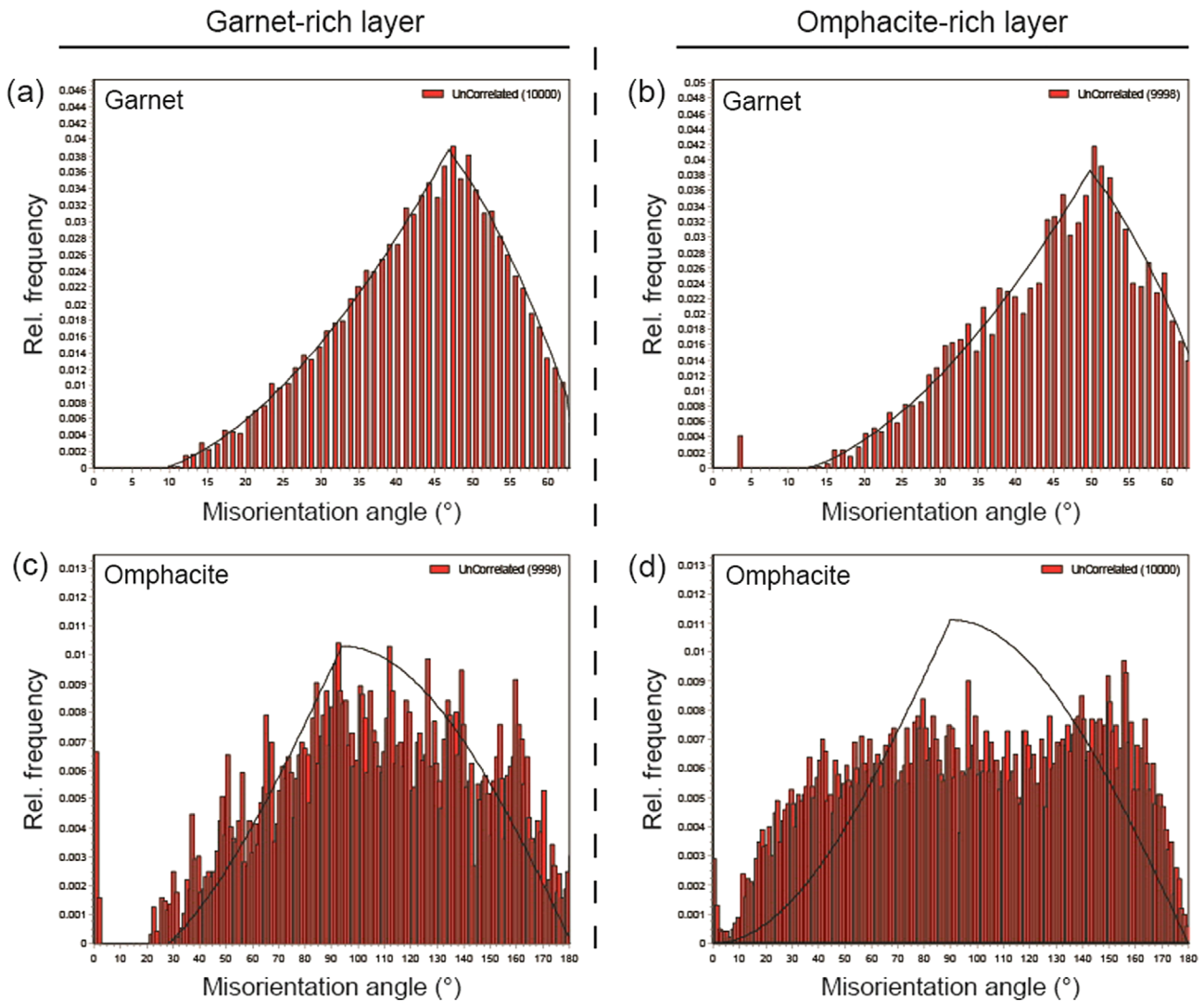


Fig. 6. Misorientation angles of uncorrelated grains. Solid lines indicate the misorientation distribution for a random fabric.

first combined data from X-ray maps with EPMA point analysis. Based on the proportionality between the quantitative (spot analyses) and X-ray intensities, we converted each mapped pixel into the oxide weight percent normalized to 100. Our preliminary calculation is only semi-quantitative, and gives ‘pseudo-bulk rock’ compositions for the GRL and ORL, which are broadly similar to the mineral chemistries of representative garnet and omphacite, respectively (Table 1). A stoichiometric calculation of the pseudo compositions into garnet and omphacite formulae yielded $X_{\text{Grs}}^* = 0.15$ and $X_{\text{Fe}}^* = 0.56$ for the GRL, and $X_{\text{Na,ORL}}^* = 0.37$ and $X_{\text{Fe,ORL}}^* = 0.30$ for the ORL (where the asterisk denotes the pseudo composition). The compositional layering of the GRL and ORL is probably attributed to an inherited structure from the protolith, such as layering within a gabbro (e.g., Corfu and Hartz, 2011).

The Fe-Mg exchange reaction in garnet-clinopyroxene (Powell, 1985; Ravna, 2000; Nakamura, 2009) and the jadeite-in-clinopyroxene

content (Holland, 1980) were combined to estimate P - T conditions for eclogite facies metamorphism. Pairs of garnet cores with uniform X_{Fe} values and varying grossular content, and rims of omphacite in both GRL and ORL yielded temperatures ranging from ~620 to 680 °C at 13–15 kbar, which are minimum pressures based on the jadeite contents. These results are lower grade than those from Di Vincenzo et al. (1997), but broadly similar to values estimated by Di Vincenzo et al. (2016). The jadeite contents of symplectitic diopside ($X_{\text{Jd}} = 0.05$ –0.13) replacing omphacite indicate decompression to < 8–10 kbar, although these estimates may not be reliable owing to low X_{Jd} values (Holland, 1980). The well-preserved prograde zoning of garnet and the development of omphacite CPOs defining the foliation and lineation may be related to the flow of dynamically recrystallized grains, suggesting the preservation of syn-kinematic microstructures. Therefore, the P - T conditions for the main deformation are estimated at ~620–680 °C and > 13–15 kbar.

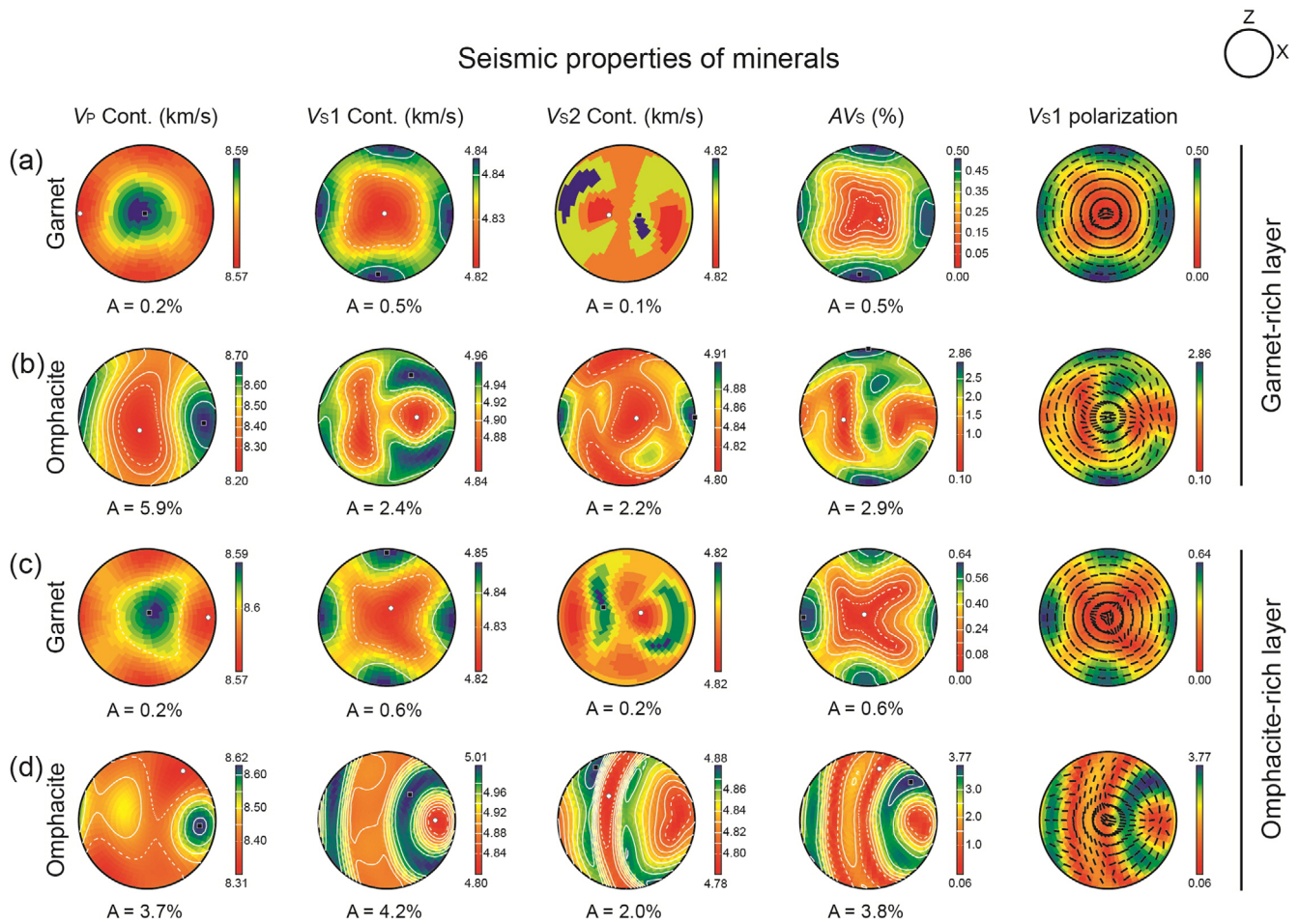


Fig. 7. Seismic properties of garnet and omphacite in each layer. Black and blank squares in each pole present maxima and minima, respectively. A: anisotropy; X: lineation; Z: foliation normal.

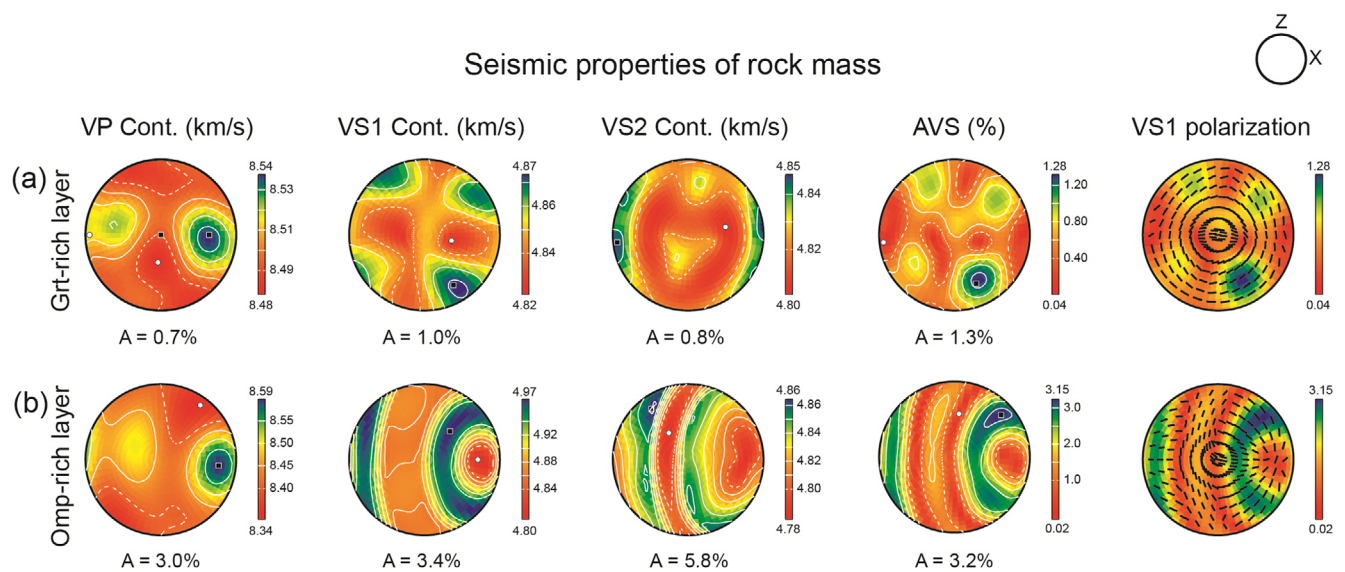


Fig. 8. Seismic properties of the garnet- and omphacite-rich layers, assuming that the whole rocks are composed only of garnet and omphacite. Symbols are as in Figure 7.

6.2. Deformation Mechanisms of Garnet and Omphacite, and the Rheology of Eclogite

Microstructures in rocks within subducting slabs are usually influenced by: (1) progressive metamorphism, where minerals transform due to changing pressure and temperature conditions; and (2) the deformation of mineral phases, which is controlled by the physical properties of the minerals and the prevailing conditions, including stress, strain, strain rate, pressure, and temperature. In this study, thin-section-scale sample analysis indicates that the formation of microstructures was controlled mainly by strain and strain rate, rather than stress, pressure, or temperature. Cataclastic deformation of rigid garnet occurs at low temperatures (e.g., Küster and Stöckhert, 1999; Trepmann and Stöckhert, 2002), whereas plastic behavior is dominant at high temperatures (e.g., Ji and Martignole, 1994; Prior et al., 2002; Mainprice et al., 2004). Garnet within both layers in this study is euhedral to subhedral, shows a uniform grain size distribution, shows a shape preferred orientation relative to the foliation without any change in both layers, yields a near-random CPO (0.002 for the *M*-index and 1.028–1.031 for the *J*-index), and misorientation angles between uncorrelated grains show a random distribution (Figs. 2, 4–6; Table 2), indicating that the garnets are largely undeformed. The relatively high aspect ratios and similar distribution for shape preferred orientation (angle to foliation) together with growth zonation of garnet in both layers could be attributed to oriented growth during the prograde-to-peak stage of metamorphism (Figs. 2c, d and 4).

In contrast, dislocation creep is commonly regarded as the dominant deformation mechanism of omphacite in eclogite (e.g., Buatier et al., 1991; Philippot and van Roermund, 1992; Godard and van Roermund, 1995; Bascou et al., 2001, 2002; Keppler et al., 2016). In this study, omphacite shows high aspect ratios (> 2.0), a strong CPO (> 0.102 for the *M*-index and > 6.573 for the *J*-index), a wide grain-size distribution, and misorientation angles between uncorrelated grains are far from a random distribution (Figs. 2, 4–6), indicating that dislocation creep was the main deformation mechanism. The existence of symplectitic clinopyroxene around the margins of omphacite suggests decompression during exhumation with concomitant structural reworking of eclogite fabric by recovery or diffusion creep. The omphacite CPOs, which can be classified as S-type based on the girdle-shaped [001] and a cluster of the [010], and L-type distinguished by the girdle of b-axes and single cluster of c-axes (after Helmstaedt et al., 1972), can be useful for indicating particular strain regimes such as flattening (S-type) and constriction (L-type) (Kurz et al., 2004; Kurz, 2005; Zhang et al., 2006). The CPOs of omphacite in the ORL are L-type, as indicated by single clusters of [001] with a girdle of (010); those in the GRL tend to

show stronger maxima of (010) orientations (Fig. 7). Based on our *P-T* estimates, deformation temperatures of ~620–680 °C are consistent with L-type (high-*T*) fabrics, or the transition from L- to S-type at ~600–900 °C (Kurz et al., 2004).

The rheology of a biminerally rock mass is usually controlled by the mechanically weak phase (e.g., Handy, 1994). Garnet is believed to be largely unaffected by deformation, and omphacite controls the rheology of eclogite by the development of a shape preferred orientation and CPO (Jin et al., 2001; Brenker et al., 2002). In this study, compared with garnet, omphacite in both layers tends to have higher aspect ratios, lower angles between crystal long axes and the foliation, a smaller grain size, higher fabric indices (*M*- and *J*-indices), and less-random misorientation angles (Figs. 4–6). In addition, compared with the ORL, garnet and omphacite in the GRL tend to exhibit higher angles between crystal long axes and the foliation, smaller grain sizes, lower aspect ratios, lower fabric indices, and near-random misorientation angles. Therefore, our results suggest strain localization into omphacite rather than garnet, confirming that omphacite controls the rheology of eclogite. Strain localization into mechanically weak phases has also been reported in experimentally and naturally deformed rocks (e.g., Zhang and Green, 2007; Kim et al., 2013b; Kim et al., 2015).

6.3. Seismic Properties

High-pressure metamorphic rocks often act as a window for internal structures beneath subduction zone (e.g., Cao et al., 2013; Cao and Jung, 2016) hence calculations on seismic properties of every eclogite could give precious information due to its rare occurrence as outcrops. To better understand seismic properties

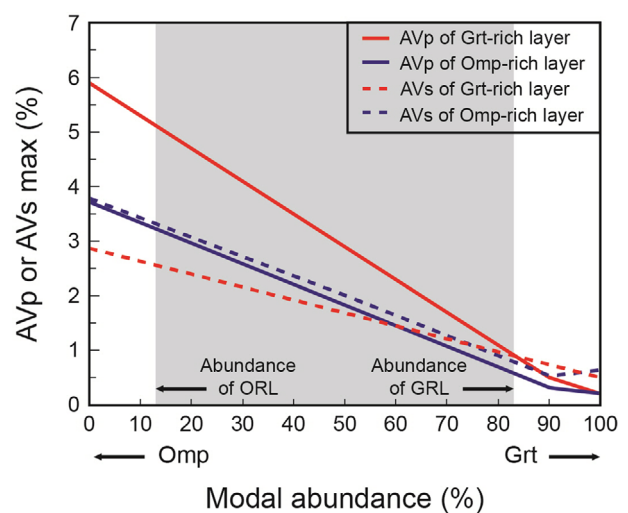


Fig. 9. Maximum P- and S-wave anisotropies (AV_p and AV_s) according to the modal abundances (vol%) of garnet and omphacite. The values were calculated each 10% step in modal abundance.

of the studied eclogite, the AV_P and AV_S values of the sample, determined based on the modal abundance of garnet and omphacite, are shown in Figure 9. Due to the near-isotropic and anisotropic characteristics of garnet and omphacite, respectively, the seismic properties of eclogite are strongly dependent on the abundance of omphacite. The linear AV_P and AV_S trends in Figure 9 show a change in slope corresponding to an ORL composition of 90% garnet and 10% omphacite. The AV_S trend is attributed to the different propagation directions of garnet and omphacite (e.g., Kim et al., 2013b). To compare the seismic anisotropy of garnet and omphacite in the Lanterman eclogite, Figure 10 shows data for different thicknesses of an anisotropic layer composed of single minerals (e.g., Satsukawa et al., 2010,

2011), along with data for olivine (Katayama and Karato, 2006) and serpentine (Katayama et al., 2009) for comparison. The thickness (D) of the anisotropic layer can be defined from $dt = AV_S / \langle V_S \rangle D$, where dt is the delay time, AV_S is the anisotropy of a specific propagation direction, and $\langle V_S \rangle$ is the average of the fast and slow velocities. Based on the results of this study, the calculated layer thicknesses are 166–212 km for garnet and 37–38 km for omphacite. Compared with the thicknesses obtained for serpentine (3 km) and olivine (23 km), the seismic anisotropy generated by eclogite partially generates to that measured in subduction zones.

The seismic anisotropy of eclogite is generally controlled by omphacite rather than garnet, based on their mechanical properties. The seismic properties of garnet polycrystals, as calculated in this study, show V_P of 8.57–8.59 km/s and V_S of 4.82–4.85 km/s, with AV_S of 0.50–0.64% (Fig. 7); these values are slightly lower than the values of 8.99–9.15 km/s, 5.16–5.36 km/s and 3.69%, respectively, reported by Zhang and Green (2007). Omphacite polycrystals of the present study exhibit V_P of 8.20–8.70 km/s, V_S of 4.80–5.01 km/s, and AV_S of 2.86–3.77%, generally lower than the values of 8.99–9.15 km/s, 5.16–5.36 km/s, and 3.69%, respectively, reported by Zhang and Green (2007). The seismic properties of eclogite that is composed dominantly of garnet and omphacite show V_P of 8.34–8.59 km/s, V_S of 4.78–4.97 km/s, and AV_S of 1.28–3.15% (Fig. 8). In particular, the seismic properties of the ORL show an increase of 329% for AV_P and 146% for AV_S relative to the GRL. Comparing these results with previous studies, shear wave splitting of the ORL calculated in this study shows an increase of at least 25% (Table 3). Glaucophane-rich layers in layered blueschists show similar increases of 87% for AV_P and 100% for AV_S relative to lawsonite-rich layers (Kim et al., 2013a). Thus, our results suggest a

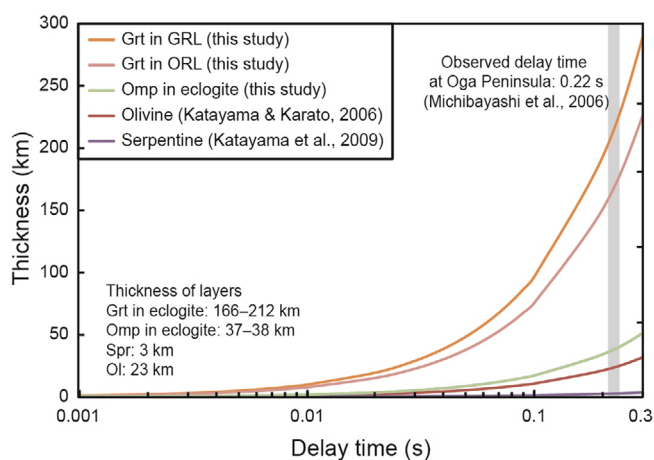


Fig. 10. Thickness of an anisotropic layer of various compositions versus delay time. The thickness and delay time of an anisotropic layer of serpentine ($AV_S = 35.9\%$, $\langle V_S \rangle = 4.13$ km/s; Katayama et al., 2009) and olivine ($AV_S = 4.5\%$, $\langle V_S \rangle = 4.75$ km/s; Katayama and Karato, 2006) are plotted for comparison. The delay time employed here is from Oga Peninsula due to lack of seismic data from the study area.

Table 3. Omphacite fabrics and its seismic properties

Samples	Sample location	J -index	Mean grain size (μm)	AV_P max (%)	AV_S max (%)	P-T conditions	Omp/Grt (vol%)	Reference
GRL	Lanterman Range, northern Victoria Land, Antarctica	6.57	178	5.9 (Omp), 0.7 (rock)	2.86 (Omp), 1.3 (rock)	~620–680 °C, > 13–15 kbar	10/69	This study
ORL	Lanterman Range, northern Victoria Land, Antarctica	7.16	277	3.7 (Omp), 3.0 (rock)	3.77 (Omp), 3.2 (rock)	~620–680 °C, > 13–15 kbar	75/15	This study
ABE	Alpe Arami, Lepontine gneisses, Alpine	6.45	4000 × 1000	2.5 (rock)	1.25 (rock)	750–900 °C, 18–35 kbar	70/30	Heinrich (1986); Bascou et al. (2001, 2002)
B6	Western Gneiss Region, Nordfjord, Norway	7.74	3000 × 1000	1.2 (rock)	1.41 (rock)	650–700 °C, 14–16 kbar	60/40	Krogh (1982); Bascou et al. (2001, 2002)
S522	Gourma area, northern Mali	4.50	1500 × 800 and 400 × 200	2.9 (rock)	1.18 (rock)	700–750 °C, > 27 kbar	75/25	Caby (1994); Bascou et al. (2001, 2002)
SL50	Sulu terrain, China	6.52	3000 × 1000	1.3 (rock)	1.80 (rock)	700–890 °C, > 28 kbar	75/25	Zhang et al. (1995); Bascou et al. (2001, 2002)
D95-24	Bixiling complex, Dabie UHP terrain, China		200–500	2.0 (Omp), 1.0 (rock)		610–700 °C, > 27 kbar	50/40	Zhang et al. (1995); Zhang and Green (2007)
MB98-08	Maobei, Sulu UHP terrain, China		250–3000 long	2.5 (Omp), 1.2 (rock)		780–870 °C, 5–7 GPa	50/49	Zhang et al. (2003); Zhang and Green (2007)

significant influence of layering structure on the seismic properties of natural eclogite in subduction zones. Additional investigations considering other minerals into calculations on seismic properties are requested.

7. CONCLUSIONS

Layering structure in gabbro is common, and may be inherited during their metamorphism to eclogite, forming alternating garnet- and omphacite-rich layers. Here we analyzed the fabric of GRL and ORL in the Lanterman eclogite from the NVL, Antarctica, to assess the influence of the layered structure on the seismic properties of the rocks. Preferential strain localization into the ORL results in an increase of up to 329% in AV_p and 146% in AV_s relative to the GRL. The strain localization is attributed to the layered structure. Additional studies of layered blueschists and eclogites are essential to reveal the influence of layering on the seismic properties of subducting oceanic crust.

ACKNOWLEDGMENTS

The authors appreciate the technical supports of Changkun Park and Hwayoung Kim for the EPMA analysis, and Kyungtae Park and Heymi Cho for the EBSD analysis. This research was supported by a KOPRI project (20140409, PM18030) to Ji Lee. The authors acknowledge the editor, Raehee Han, and two anonymous reviewers for assistance and constructive comments that significantly improved the manuscript.

REFERENCES

- Ábalos, B., Fountain, D.M., Gil Ibarra, J.I., and Puelles, P., 2011, Eclogite as a seismic marker in subduction channels: seismic velocities, anisotropy, and petrofabric of Cabo Ortegal eclogite tectonites (Spain). *Geological Society of American Bulletin*, 123, 439–456.
- Armienti, P., Ghezzo, C., Innocenti, F., Manetti, P., Rocchi, S., and Tonarini, S., 1990, Isotope geochemistry and petrology of granitoid suites from Granite Harbour Intrusives of the Wilson Terrane, North Victoria Land, Antarctica. *European Journal of Mineralogy*, 2, 103–123.
- Babuška, V., Kumazawa, M., Ohno, I., and Sumino, Y., 1978, Elastic properties of garnet solid-solution series. *Physics of the Earth and Planetary Interiors*, 16, 157–176.
- Bascou, J., Barruol, G., Vauchez, A., Mainprice, D., and Egydio-Silva, M., 2001, EBSD-measured lattice-preferred orientations and seismic properties of eclogites. *Tectonophysics*, 342, 61–80.
- Bascou, J., Tommasi, A., and Mainprice, D., 2002, Plastic deformation and development of clinopyroxene lattice preferred orientations in eclogites. *Journal of Structural Geology*, 24, 1357–1368.
- Bezacier, L., Reynard, B., Bass, J.D., Wang, J., and Mainprice, D., 2010, Elasticity of glaucophane, seismic velocities and anisotropy of the subducted oceanic crust. *Tectonophysics*, 494, 201–210.
- Bhagat, S., Bass, J.D., and Smyth, J., 1992, Single-crystal elastic properties of omphacite-C2/c by Brillouin spectroscopy. *Journal of Geophysical Research*, 97, 6843–6848.
- Bomparola, R.M., Chezzo, C., Belousova, E., Griffin, W.L., and O'Reilly, S.Y., 2007, Resetting of the U-Pb Zircon System in Cambro-Ordovician Intrusives of the Deep Freeze Range, Northern Victoria Land, Antarctica. *Journal of Petrology*, 48, 327–364.
- Bradshaw, J.D. and Laird, M.G., 1983, The pre-Beacon geology of northern Victoria Land: a review. *Proceedings of the 4th SCAR/IUGS Symposium on Antarctic Earth Sciences, Adelaide, Aug. 16–20 p. 98–101.*
- Brenker, F.E., Prior, D.J., and Müller, W.F., 2002, Cation ordering in omphacite and effect on deformation mechanism and lattice preferred orientation (LPO). *Journal of Structural Geology*, 24, 1991–2005.
- Buatier, M., van Roermund, H.L.M., Drury, M.R., and Lardeaux, J.M., 1991, Deformation and recrystallization mechanisms in naturally deformed omphacites from the Sesia-Lanzo zone; geophysical consequences. *Tectonophysics*, 195, 11–27.
- Bunge, H.J., 1982, *Texture Analysis in Materials Science*. Butterworth, London, 559 p.
- Caby, R., 1994, Precambrian coesite from northern Mali: first record and implications for plate tectonics in the trans-Saharan segment of the Pan-African belt. *European Journal of Mineralogy*, 6, 235–244.
- Cao, Y., Jung, H., and Song, S., 2013, Petro-fabrics and seismic properties of blueschist and eclogite in the North Qilian suture zone, NW China: implications for the low-velocity upper layer in subducting slab, trench-parallel seismic anisotropy, and eclogite detectability in the subduction zone. *Journal of Geophysical Research*, 118, 3037–3058.
- Cao, Y., Jung, H., and Song, S., 2014, Microstructures and petro-fabrics of lawsonite blueschist in the North Qilian suture zone, NW China: implications for seismic anisotropy of subducting oceanic crust. *Tectonophysics*, 628, 140–157.
- Cao, Y. and Jung, H., 2016, Seismic properties of subducting oceanic crust: Constraints from natural lawsonite-bearing blueschist and eclogite in Sivrihisar Massif, Turkey. *Physics of the Earth and Planetary Interiors*, 250, 12–30.
- Corfu, F. and Hartz, E.H., 2011, U-Pb geochronology in Liverpool Land and Canning Land, East Greenland – the complex record of a polyphase Caledonian orogeny. *Canadian Journal of Earth Sciences*, 48, 473–494.
- Crispini, L., Di Vincenzo, G., and Palmeri, R., 2007, Petrology and Ar-Ar dating of shear zones in the Lanterman Range (northern Victoria Land, Antarctica): implications for metamorphic and temporal evolution at terrane boundaries. *Mineralogy and Petrology*, 89, 217–249.
- Di Vincenzo, G., Palmeri, R., Talarico, F., Andriessen, P.A.M., and Ricci, C.A., 1997, Petrology and geochronology of eclogites from the Lanterman Range, Antarctica. *Journal of Petrology*, 38, 1391–1417.
- Di Vincenzo, G. and Palmeri, R., 2001, An $^{40}\text{Ar}/^{39}\text{Ar}$ investigation of high-pressure metamorphism and the retrogressive history of mafic eclogites from the Lanterman Range (Antarctica): evidence against a simple temperature control on argon transport in amphi-

- bole. *Contributions to Mineralogy and Petrology*, 141, 15–35.
- Di Vincenzo, G., Ghiribelli, B., Giorgetti, G., and Palmeri, R., 2001, Evidence of a close link between petrology and isotope Records; constraints from SEM, EMP, TEM and in situ $^{40}\text{Ar}/^{39}\text{Ar}$ laser analyses on multiple generations of white micas (Lanternman Range, Antarctica). *Earth Planetary Science Letters*, 192, 389–405.
- Di Vincenzo, G., Horton, F., and Palmeri, R., 2016, Protracted (~30 Ma) eclogite-facies metamorphism in northern Victoria Land (Antarctica): implications for the geodynamics of the Ross/Delamerian Orogen. *Gondwana Research*, 40, 91–106.
- Fujimoto, Y., Kono, Y., Hirajima, T., Kanagawa, K., Ishikawa, M., and Arima, M., 2010, P-wave velocity and anisotropy of lawsonite and epidote blueschists: constraints on water transportation along subducting oceanic crust. *Physics of the Earth and Planetary Interiors*, 183, 219–228.
- Godard, G., 2001, Eclogites and their geodynamic interpretation: a history. *Journal of Geodynamics*, 32, 165–203.
- Godard, G. and Palmeri, R., 2013, High-pressure metamorphism in Antarctica from the Proterozoic to the Cenozoic: a review and geodynamic implications. *Gondwana Research*, 23, 844–864.
- Godard, G. and van Roermund, H.L.M., 1995, Deformation-induced clinopyroxene fabrics from eclogites. *Journal of Structural Geology*, 17, 1425–1443.
- Ghiribelli, B., Frezzotti, M.-L., and Palmeri, R., 2002, Coesite in eclogites of the Lanterman Range (Antarctica): evidence from textural and Raman studies. *European Journal of Mineralogy*, 14, 355–360.
- Ha, Y., Jung, H., and Raymond, L.A., 2018, Deformation fabrics of glaucophane schists and implications for seismic anisotropy: the importance of lattice preferred orientation of phengite. *International Geology Review*. <https://doi.org/10.1080/00206814.2018.1449142>
- Handy, M.R., 1994, Flow laws for rocks containing two non-linear viscous phases: a phenomenological approach. *Journal of Structural Geology*, 16, 287–301.
- Heinrich, C.A., 1986, Eclogite facies regional metamorphism of hydrous mafic rocks in the Central Alpine Adula Nappe. *Journal of Petrology*, 27, 123–154.
- Helmstaedt, H., Anderson, O., and Gavasci, A., 1972, Petrofabric studies of eclogite, spinel-websterite and spinel-lherzolite xenoliths from kimberlite-bearing breccia pipes in Southeastern Utah and Northeastern Arizona. *Journal of Geophysical Research*, 47, 4350–4365.
- Holland, T.J.B., 1980, The reaction albite = jadeite + quartz determined experimentally in the range 600–1200 °C. *American Mineralogist*, 65, 129–134.
- Ji, S. and Martignole, J., 1994, Ductility of garnet as an indicator of extremely high temperature deformation. *Journal of Structural Geology*, 16, 985–996.
- Ji, S., Saruwatari, K., Mainprice, D., Wirth, R., Xu, Z., and Xia, B., 2003, Microstructures, petrofabrics and seismic properties of ultra high-pressure eclogites from Sulu region, China: implications for rheology of subducted continental crust and origin of mantle reflections. *Tectonophysics*, 370, 49–76.
- Jin, Z.-M., Zhang, J., Green, H.W., and Jin, S., 2001, Eclogite rheology: implications for subducted lithosphere. *Geology*, 99, 667–670.
- Katayama, I. and Karato, S.-I., 2006, Effect of temperature on the B- to C-type olivine fabric transition and implication for flow pattern in the subduction zone. *Physics of the Earth and Planetary Interiors*, 157, 33–45.
- Katayama, I., Hirauchi, K., Michibayashi, K., and Ando, J., 2009, Trench-parallel anisotropy produced by serpentine deformation in the hydrated mantle wedge. *Nature*, 461, 1114–1117.
- Keppler, R., Ullemeyer, K., Behrmann, J.H., Stipp, M., Kurzwski, R.M., and Lokajčiček, T., 2015, Crystallographic preferred orientations of exhumed subduction channel rocks from the Eclogite Zone of the Tauern Window (Eastern Alps, Austria), and implications on rock elastic anisotropies at great depths. *Tectonophysics*, 647–648, 89–104.
- Keppler, R., Stipp, M., Behrmann, J.H., Ullemeyer, K., and Heidelbach, F., 2016, Deformation inside a paleosubduction channel – insights from microstructures and crystallographic preferred orientations of eclogites and metasediments from the Tauern Window, Austria. *Journal of Structural Geology*, 82, 60–79.
- Kim, D., Katayama, I., Michibayashi, K., and Tsujimori, T., 2013a, Rheological contrast between glaucophane and lawsonite in naturally deformed blueschist from Diablo range, California. *Island Arc*, 22, 63–73.
- Kim, D., Katayama, I., Michibayashi, K., and Tsujimori, T., 2013b, Deformation fabrics of natural blueschists and implications for seismic anisotropy in subducting oceanic crust. *Physics of the Earth and Planetary Interiors*, 444, 8–21.
- Kim, D., Katayama, I., Wallis, S., Michibayashi, K., Miyake, A., Seto, Y., and Azuma, S., 2015, Deformation microstructures of glaucophane and lawsonite in experimentally deformed blueschists: implications for intermediate-depth intraplate earthquakes. *Journal of Geophysical Research*, 120, 1229–1242.
- Kim, D., Wallis, S., Endo, S., and Ree, J.-H., 2016, Seismic properties of lawsonite eclogites from the southern Motagua fault zone, Guatemala. *Tectonophysics*, 677–678, 88–98.
- Krogh, E.J., 1982, Metamorphic evolution deduced from mineral inclusions and compositional zoning in garnets from Norwegian country-rock eclogites. *Lithos*, 15, 305–321.
- Kurz, W., Jansen, E., Hundernborn, R., Pleuger, J., Schäfer, W., and Unzog, W., 2004, Microstructures and crystallographic preferred orientations of omphacite in Alpine eclogites: implications for the exhumation of (ultra-) high-pressure units. *Journal of Geodynamics*, 37, 1–55.
- Kurz, W., 2005, Constriction during exhumation: evidence from eclogite microstructures. *Geology*, 33, 37–40.
- Küster, M. and Stöckhert, B., 1999, High differential stress and sub-lithostatic pore fluid pressure in the ductile regime – microstructural evidence for short term postseismic creep in the Sesia Zone, Western Alps. *Tectonophysics*, 303, 263–277.
- Leake, B.E., Woolley, A.R., Arps, C.E.S., Birch, W.D., Gilbert, M.C., Grice, J.D., Hawthorne, F.D., Kato, A., Kisch, H.J., Krivovichev, V.G., Linthout, K., Laird, J., Mandarino, J.A., Maresch, W.V., Nickel, E.H., Rock, N.M.S., Schumacher, J.C., Smith, D.C., Stephenson, N.C.N., Ungaretti, L., Whittaker, E.J.W., and Youzhi, G., 1997, Nomenclature of amphiboles: report of the subcommittee on amphiboles of the international mineralogical association, commission on new minerals and mineral names. *The Canadian Mineralogist*, 35, 219–246.
- Mainprice, D., 1990, A Fortran program to calculate seismic anisot-

- ropy from the lattice preferred orientation of minerals. *Computers & Geosciences*, 16, 385–393.
- Mainprice, D. and Silver, P.G., 1993, Interpretation of SKS-waves using samples from the subcontinental lithosphere. *Physics of the Earth and Planetary Interiors*, 78, 257–280.
- Mainprice, D., Barruol, G., and Ben Ismail, W., 2000, The anisotropy of the Earth's mantle: from single crystal to polycrystal. In: Karato, S., Forte, A.M., Liebermann, R.C., Masters, G., and Stixrude, L. (eds.), *Earth's Deep Interior: Mineral Physics and Tomography from the Atomic to the Global Scale*. Geophysical Monograph Series, 117, p. 237–264.
- Mainprice, D., Bascou, J., Cordier, P., and Tommasi, A., 2004, Crystal preferred orientations of garnet: comparison between numerical simulations and electron back-scattered diffraction (EBSD) measurements in naturally deformed eclogites. *Journal of Structural Geology*, 26, 2089–2102.
- Mainprice, D., Hielscher, R., and Schaeben, H., 2011, Calculating anisotropic physical properties from texture data using the MTEX open source package. In: Prior, D.J., Rutter, E.H., and Tatham, D.J. (eds.), *Deformation Mechanisms, Rheology and Tectonics: Microstructures, Mechanics and Anisotropy*. Geological Society, London, Special Publications, 360, p. 175–192.
- Mezger, J.E., 2010, Rotation of irregular staurolite porphyroblasts in a simple shear dominated shear zone controlled by initial growth orientation and aspect ratio. *Journal of Structural Geology*, 32, 1147–1157.
- Michibayashi, K., Abe, N., Okamoto, A., Satsukawa, T., and Michikura, K., 2006, Seismic anisotropy in the uppermost mantle, back-arc region of the northeast Japan arc: petrophysical analyses of Ichinomegata peridotite xenoliths. *Geophysical Research Letters*, 33, L10312. <https://doi.org/10.1029/2006GL025812>
- Morales, L.F.G. and Tommasi, A., 2011, Composition, textures, seismic and thermal anisotropies of xenoliths from a thin and hot lithospheric mantle (Summit Lake, southern Canadian Cordillera). *Tectonophysics*, 507, 1–15.
- Morimoto, N., 1988, Nomenclature of pyroxenes. *Mineralogical Magazine*, 52, 535–550.
- Nakamura, D., 2009, A new formulation of garnet-clinopyroxene geothermometer based on accumulation and statistical analysis of a large experimental data set. *Journal of Metamorphic Geology*, 27, 495–508.
- Palmeri, R., Ghiribelli, B., Ranalli, G., Talarico, F., and Ricci, C.-A., 2007, Ultrahigh-pressure metamorphism and exhumation of garnet-bearing ultramafic rocks from the Lanterman Range (northern Victoria Land, Antarctica). *Journal of Metamorphic Geology*, 25, 225–243.
- Palmeri, R., Frezzotti, M.L., Godard, G., and Davies, J., 2009, Pressure-induced incipient amorphization of α -quartz and transition to coesite in an eclogite from Antarctica: a first record and some consequences. *Journal of Metamorphic Geology*, 27, 685–705.
- Palmeri, R., Talarico, F.M., and Ricci, C.A., 2011, Ultrahigh-pressure metamorphism at the Lanterman Range (northern Victoria Land, Antarctica). *Geological Journal*, 46, 126–136.
- Philippot, P. and Van Roermund, L.M., 1992, Deformation processes in eclogitic rocks: evidence for the rheological delamination of the oceanic crust in deeper levels of subduction zones. *Journal of Structural Geology*, 14, 1059–1077.
- Powell, R., 1985, Regression diagnostics and robust regression in geothermometer/geobarometer calibration: the garnet-clinopyroxene geothermometer revisited. *Journal of Metamorphic Geology*, 3, 231–243.
- Prior, D.J., Wheeler, J., Peruzzo, L., Spiess, R., and Storey, C., 2002, Some garnet microstructures: an illustration of the potential of orientation maps and misorientation analysis in microstructural studies. *Journal of Structural Geology*, 24, 999–1001.
- Ravna, E.K., 2000, The garnet-clinopyroxene Fe^{2+} -Mg geothermometer: an updated calibration. *Journal of Metamorphic Geology*, 18, 211–219.
- Ricci, C.A., Talarico, F., Palmeri, R., Di Vincenzo, G., and Pertusati, P.C., 1996, Eclogite at the Antarctic palaeo-Pacific active margin of Gondwana (Lanterman Range, northern Victoria Land, Antarctica). *Antarctic Science*, 8, 277–280.
- Ricci, C.A., Talarico, F., and Palmeri, R., 1997, Tectonothermal evolution of the Antarctic Pale-Pacific active margin of Gondwana; a northern Victoria Land perspective. *Proceedings of the VII international symposium on Antarctic earth sciences, Siena, Sep. 10–15*, p. 213–218.
- Rocchi, S., Tonarini, S., Armienti, P., Innocenti, F., and Manetti, P., 1998, Geochemical and isotopic structure of the early Paleozoic active margin of Gondwana in northern Victoria Land, Antarctica. *Tectonophysics*, 284, 261–281.
- Skemer, P., Katayama, I., Jiang, Z., and Karato, S.-I., 2005, The misorientation index: development of a new method for calculating the strength of lattice-preferred orientation. *Tectonophysics*, 411, 157–167.
- Satsukawa, T., Michibayashi, K., Raye, U., Anthony, E.Y., Pulliam, J., and Stern, R., 2010, Uppermost mantle anisotropy beneath the southern Laurentian margin: evidence from Knippa peridotite xenoliths, Texas. *Geophysical Research Letters*, 37, L20312. <https://doi.org/10.1029/2010GL044538>
- Satsukawa, T., Michibayashi, K., Anthony, E.Y., Stern, R., Gao, S.S., and Liu, K.H., 2011, Seismic anisotropy of the uppermost mantle beneath the Rio Grande rift: evidence from Kilbourne Hole peridotite xenoliths, New Mexico. *Earth and Planetary Science Letters*, 311, 172–181.
- Talarico, F., Ghiribelli, B., Smith Siddoway, C., Palmeri, R., and Ricci, C.A., 1998, The northern Victoria Land segment of the Antarctic paleo-Pacific margin of eastern Gondwana: new constraints from the Lanterman and Mountaineer Ranges. *Terra Antarctica*, 5, 245–252.
- Trepmann, C.A. and Stöckhert, B., 2002, Cataclastic deformation of garnet: a record of synseismic loading and postseismic creep. *Journal of Structural Geology*, 24, 1845–1856.
- Weaver, S.D., Bradshaw, J.D., and Laird, M.G., 1984, Geochemistry of Cambrian volcanics of the Bowers Supergroup and implications for the Early Paleozoic tectonic evolution of northern Victoria Land, Antarctica. *Earth and Planetary Science Letters*, 68, 128–140.
- Whitney, D.L. and Evans, B.W., 2010, Abbreviations for names of rock-forming minerals. *American Mineralogist*, 95, 185–187.
- Whitney, D.L., Teyssier, C., Seaton, N.C.A., and Fornash, K.F., 2014, Petrofabrics of high-pressure rocks exhumed at the slab-mantle interface from the “point of no return” in a subduction zone (Sivri-

- hisar, Turkey). *Tectonics*, 33, 2315–2341.
- Worthington, J.R., Hacker, B.R., and Zandt, G., 2013, Distinguishing eclogite from peridotite: EBSD-based calculations of seismic velocities. *Geophysical Journal International*, 193, 489–505.
- Zhang, J. and Green, H.W., 2007, On the deformation of UHP eclogite: from laboratory to nature. *International Geology Review*, 49, 487–503.
- Zhang, J., Green, H.W., and Biozhilov, K.N., 2006, Rheology of omphacite at high temperature and pressure and significance of its lattice preferred orientations. *Earth and Planetary Science Letters*, 246, 432–443.
- Zhang, J.F., Wang, Y.F., and Jin, Z.M., 2008, CPO-induced seismic anisotropy in UHP eclogites. *Science in China Series D-Earth Sciences*, 51, 11–21.
- Zhang, R., Liou, J.G., and Cong, B.L., 1995, Talc-bearing, magnesite-bearing, and Ti-clinohumite-bearing ultrahigh-pressure meta- mafic and ultramafic complex in the Dabie Mountains, China. *Journal of Petrology*, 36, 1011–1037.
- Zhang, R., Liou, J.G., Yang, J.S., and Ye, K., 2003, Ultrahigh-pressure metamorphism in the forbidden zone: the Xugou garnet peridotite, Sulu terrane, eastern China. *Journal of Metamorphic Geology*, 21, 539–550.